



## RESEARCH ARTICLE

10.1029/2023EA002958

### Key Points:

- Marine crustal magnetic anomaly maps are typically constructed from trackline data with variable uncertainties and spatial configurations
- This paper presents a methodology for creating data grids with associated cell by cell uncertainty from marine trackline data
- The method is tested against newly collected modern airborne magnetic data

### Correspondence to:

R. W. Saltus,  
richard.saltus@colorado.edu

### Citation:

Saltus, R. W., Chulliat, A., Meyer, B., Bates, M., & Sirohey, A. (2023). Magnetic anomaly grid and associated uncertainty from marine trackline data: The Caribbean Alternative Navigation Reference Experiment (CANREx). *Earth and Space Science*, 10, e2023EA002958. <https://doi.org/10.1029/2023EA002958>

Received 30 MAR 2023

Accepted 17 OCT 2023



### Author Contributions:

**Conceptualization:** R. W. Saltus, A. Chulliat, B. Meyer  
**Data curation:** R. W. Saltus, B. Meyer  
**Formal analysis:** R. W. Saltus  
**Funding acquisition:** R. W. Saltus, A. Chulliat  
**Investigation:** R. W. Saltus, A. Chulliat, B. Meyer, M. Bates  
**Methodology:** R. W. Saltus  
**Project Administration:** A. Chulliat  
**Software:** R. W. Saltus, A. Sirohey  
**Supervision:** R. W. Saltus, A. Chulliat  
**Validation:** R. W. Saltus  
**Visualization:** R. W. Saltus

© 2023 The Authors. Earth and Space Science published by Wiley Periodicals LLC on behalf of American Geophysical Union.

This is an open access article under the terms of the [Creative Commons Attribution-NonCommercial-NoDerivs License](https://creativecommons.org/licenses/by/4.0/), which permits use and distribution in any medium, provided the original work is properly cited, the use is non-commercial and no modifications or adaptations are made.

# Magnetic Anomaly Grid and Associated Uncertainty From Marine Trackline Data: The Caribbean Alternative Navigation Reference Experiment (CANREx)

R. W. Saltus<sup>1,2</sup> , A. Chulliat<sup>1,2</sup> , B. Meyer<sup>2</sup>, M. Bates<sup>3</sup>, and A. Sirohey<sup>3</sup>

<sup>1</sup>Cooperative Institute for Research in the Environmental Sciences, University of Colorado, Boulder, CO, USA, <sup>2</sup>NOAA National Centers for Environmental Information, Boulder, CO, USA, <sup>3</sup>Sander Geophysics Ltd., Ottawa, ON, Canada

**Abstract** Crustal magnetic anomaly maps over oceanic regions are based largely on marine trackline surveys. These surveys, collected from the 1950s to the present, span a wide range of data quality and reliability. We discuss a methodology for constructing grids from these data with associated cell by cell estimates of grid uncertainty. The method is tested with a modern airborne survey for a representative region in the eastern Caribbean. The results are promising, producing an uncertainty estimate that is accurate to one standard deviation for the test area. As magnetic anomaly maps and grids are increasingly applied as constraints for geologic interpretation as well as for alternative navigation (e.g., navigation by magnetic field patterns in the absence of GPS), it is important to quantify the accuracy of these maps.

**Plain Language Summary** It is challenging to make maps of the variations in the Earth's magnetic field, called crustal magnetic anomalies, caused by the distribution of magnetic minerals in oceanic areas. The reason for this is that the best available data for most marine areas is from ship-based measurements collected over many decades, from the 1950s to the present. The spatial distribution of these marine survey tracklines is highly variable as is their original data quality and reliability. Previous grids and maps constructed from marine trackline data have not included systematic estimation of the grid/map uncertainty. At best, earlier maps have included generalized statements about the estimated mean uncertainty. In this study, we present a methodology for estimating the crustal magnetic anomaly and the associated uncertainty from marine trackline data. The method is evaluated using a modern airborne survey of a test area in the eastern Caribbean, an area surrounding St. Croix in the US Virgin Islands.

## 1. Introduction

Magnetic maps depict spatial variations in the Earth's magnetic field. These variations occur at a range of scales and are produced by geophysical processes and factors, including the structure and evolution of the Earth's core field, and the geologic distribution of magnetic minerals in the lithosphere. Mankind has produced magnetic maps for 100s of years with increasing fidelity and accuracy and there is a general understanding, among the geophysicists who produce and use these maps, of the approximate resolution and accuracy of these maps. However, few magnetic maps, or the digital grids that underpin these maps, have been produced with explicit quantification of map uncertainty. In the rare instances when map uncertainty is addressed, it is typically a statistical representation at the grid or survey level and not at the individual grid cell level. For example, for the global magnetic anomaly grid EMAG2v3 (Meyer, Chulliat, & Saltus, 2017), the authors cited  $\pm 100$  nT as the average uncertainty for grid values in oceanic areas.

As magnetic maps and grids are often used in complex inversions and in combination with other data or constraints (e.g., for deriving geothermal heat flux; Kolster et al., 2023), including in machine learning applications, it is increasingly important to understand the uncertainties in these products. An example of an application with need for detailed uncertainty estimation is the use of magnetic map information for alternative navigation (Canciani, 2016; Canciani & Raquet, 2016). In this application, measurements from an onboard magnetometer are compared with previously mapped (or modeled) magnetic variations. Alternative navigation capability is important for subsea navigation and as backup to GPS and other systems. The uncertainty of the mapped information has implications for the accuracy of magnetic navigation.

Writing – original draft: R. W. Saltus  
Writing – review & editing: R. W. Saltus, A. Chulliat, B. Meyer, M. Bates

Factors that contribute to magnetic map uncertainty include (but are not limited to): vintage and type of original measured data (pre-GPS data are particularly subject to uncertainty in measurement location); spatial distribution of measured data; expectation of magnetic variability (e.g., geologic or geochemical environment); availability of redundant measurement; and the spatial scale/resolution of the magnetic map or model. Amante (2018) addressed similar issues for uncertainty estimation of digital elevation models. Preliminary reports on our approach were presented as meeting abstracts (Saltus et al., 2020, 2021a, 2021b).

In this paper we report on a hybrid approach to estimating the uncertainty in magnetic maps produced from marine trackline data. Marine magnetic trackline data are the primary input for magnetic anomaly values in the oceanic regions of global magnetic anomaly grids (e.g., EMAG2 of Meyer, Chulliat, & Saltus, 2017; Meyer, Saltus, & Chulliat, 2017, and WDMAM of Korhonen et al., 2007; Lesur et al., 2016). We apply our approach in a study area located in the vicinity of the US Virgin Islands (USVI) in the Caribbean Sea (Figure 1). The area was selected as representative of a number of analog marine regions at similar latitudes and for ease of logistics during the pandemic era. The overall project is called the Caribbean Alternative Navigation Reference Experiment (CANREx). The CANREx trackline magnetic map and associated uncertainty estimates are verified by comparison with a modern aeromagnetic survey. The results are encouraging: mapping and uncertainty estimates match the modern survey to within one sigma standard deviation. We conclude with a discussion of further work and the challenges for extending this work globally.

A quick note on use of the terms error and uncertainty in this paper. Error refers to the difference between an estimated value and a value considered to be true. Errors may be positive or negative. Uncertainty refers to the expected error range for a value that is estimated when the true value is unknown. Uncertainty is an absolute value and the expected error range is  $\pm$ uncertainty.

## 2. Data

The source data for CANREx are extracted from the Trackline Geophysics database of the NOAA National Centers for Environmental Information (NCEI, formerly known as NGDC, the National Geophysical Data Center). NCEI (and formerly NGDC) has assembled and curated magnetic trackline data collected over the past 70+ years by more than 100 institutions. The geophysical trackline data are available to the public through an online portal (<https://www.ncei.noaa.gov/maps/trackline-geophysics/>).

Data were extracted from the NCEI database for the CANREx region, spanning from 16° to 20° in latitude and –62° to –68° in longitude. The tracklines include data from 60 separate cruises collected by 10 agencies over a span of 57 years from 1959 to 2012 (Table 1). The tracklines have an irregular geometry within the study area (Figure 2); this is typical of most marine regions.

Initial processing of the trackline magnetic data followed the procedure established for EMAG2v3 (Meyer, Chulliat, & Saltus, 2017). Key aspects of this processing include: (a) initial basic quality control, (b) consistent recalculation of crustal field anomalies using core field and external field models appropriate to the survey data epoch, and (c) exclusion of data with extreme values ( $>1,000$  or  $<-1,000$ ), gradients ( $>100$  nT/km or  $<-100$  nT/km), or that were collected during periods of magnetic disturbance ( $K_p$  index greater than 60).

EMAG2v3 utilized a kriging methodology for grid production (Meyer, Chulliat, & Saltus, 2017) with a generalized spherical semivariogram model applied on a regional basis. The parameters defining the spherical semivariogram model for EMAG2v3 were taken as default values from a simple semivariogram curve fitting algorithm in the Oasis montaj software used for the gridding.

Application of a kriging methodology, using default spherical fit parameters, to the trackline magnetic data produces a magnetic anomaly grid (depicted in Figure 3) and associated uncertainty estimate grid (Figure 4). The applied semivariogram model, based on a default algorithm, is a spherical function with a nugget value (mean uncertainty of cell data) of 30 nT, a range (typical distance over which anomaly values are correlated) of 560 km, and a sill (maximum uncertainty) of 150 nT.

In practice, the overall magnetic anomaly pattern as seen in Figure 3 is relatively invariant with respect to gridding methodology at the cell size of 4 km for this marine trackline distribution. For example, a grid constructed using the minimum curvature algorithm versus a kriging algorithm will look broadly similar. Robust features of these grids for this area include the broad east-west zone of negative values in the northern part of the study area,

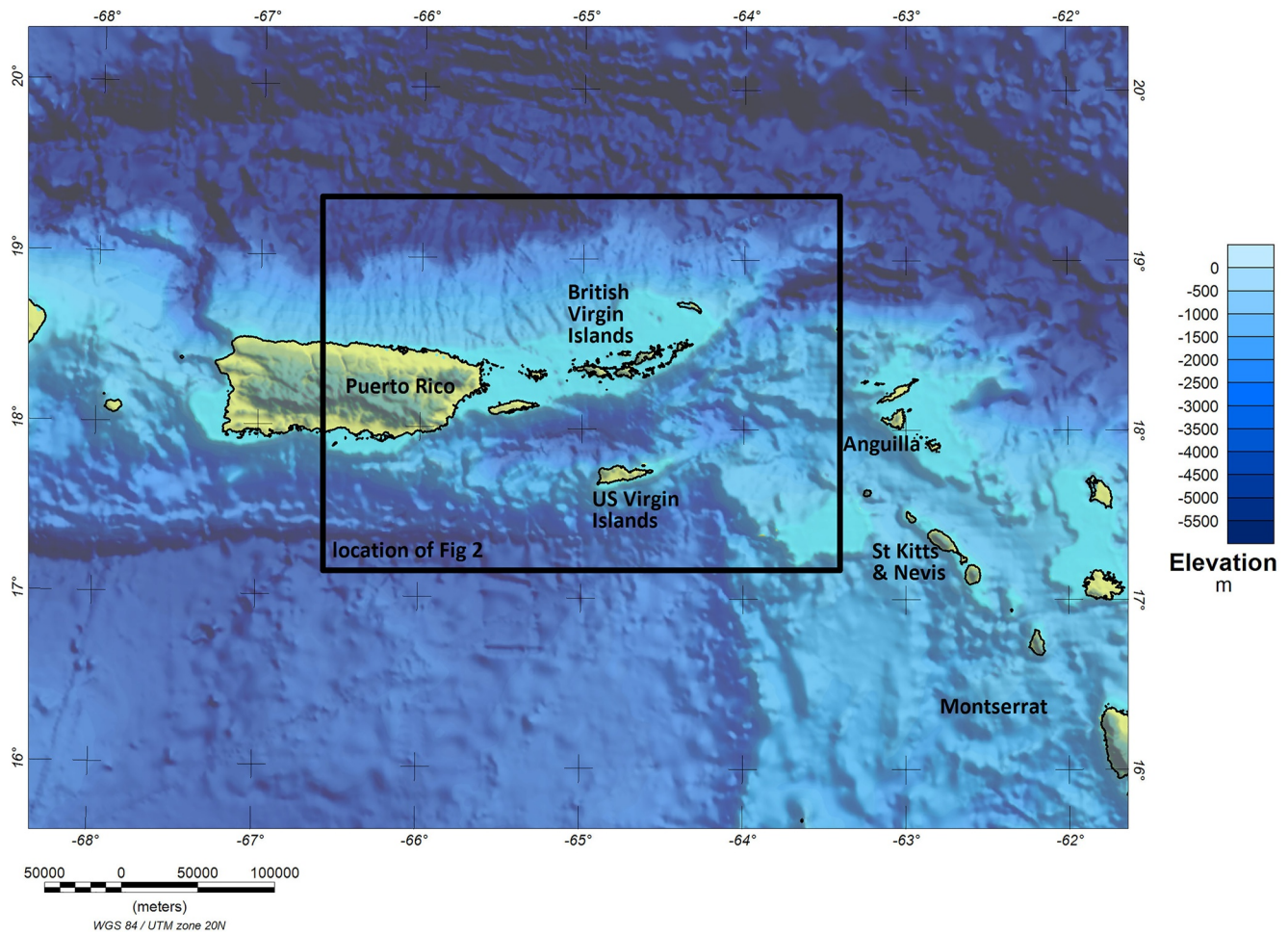


**Figure 1.** Location map of the Caribbean Alternative Navigation Reference Experiment study area. The black box indicates the study area (and the extent of Figure 2 and subsequent map figures). Background shaded relief image depicts SRTM30 global bathymetry (Becker et al., 2009).

a zone of higher values spanning the central island platform, a relatively neutral zone with smaller variations in the southwest portion, and a zone of variable highs and lows in the southeast corner. Overall magnetic anomaly values range between  $\pm 200$  nT.

The default semivariogram model (Figure 4) applied to this grid features a “generous” estimate of expected anomaly correlation, expressed as a large range value over 500 km. This results in a smoothing of the 4 km cell size as data with significant distance from the grid cell can still influence the grid cell value. This smoothing has the benefit of averaging out data errors, but with the downside of reducing grid resolution.

### 3. Methodology

Our approach begins with the assignment of pointwise uncertainty estimates to the trackline magnetic anomaly values. Sources of uncertainty for these measurements include, but are not limited to, inaccurate positioning (especially true for pre-GPS cruises), lack of diurnal corrections, magnetic disturbance from the ship, as well as instrumental factors such as drift, calibration, and accuracy. It is not possible to precisely determine these factors, particularly for surveys lacking complete metadata. Our approach for this experiment is to assign general uncertainty to the trackline surveys based on the age of the survey as listed in Table 1. The values assigned are based on practical experience of the authors as well as spot checks of crossing errors for surveys based on the era of data collection. The uncertainty difference for pre/post 1980 is based on transition from older forms of marine navigation to GPS. The break at year 2000 is related to better processing models available from satellite data.

**Table 1**  
*Summary of National Centers for Environmental Information Trackline Data Extracted in the Caribbean Alternative Navigation Reference Experiment Study Area*

| Survey ID | Agency  | Ship              | Date   | Number of points | Data min (nT) | Data max (nT) | Data mean (nT) | Data standard deviation (nT) |
|-----------|---------|-------------------|--------|------------------|---------------|---------------|----------------|------------------------------|
| V1603     | Lamont  | Vema              | 1959.8 | 84               | 130.2         | 398.2         | 229.3          | 63.8                         |
| RC0801    | Lamont  | Conrad            | 1963.9 | 77               | -113.6        | 332.9         | 54.8           | 86.7                         |
| RC0809    | Lamont  | Conrad            | 1964.4 | 401              | -284.7        | 452.3         | -37            | 78.2                         |
| RC0812    | Lamont  | Conrad            | 1964.6 | 71               | -254.3        | 121.9         | -74.2          | 83                           |
| OPR470    | NOAA    | Discoverer        | 1966.8 | 113              | -288.8        | 1.6           | -178           | 68.9                         |
| V2413     | Lamont  | Vema              | 1967.9 | 118              | -163.1        | 15.8          | -67.6          | 46.5                         |
| AMC0168   | NOAA    | Discoverer        | 1968   | 247              | -248.6        | 37.9          | -71.5          | 67.3                         |
| V2607     | Lamont  | Vema              | 1969.2 | 285              | -285.7        | 569.1         | -33.1          | 156.3                        |
| LY70B     | US Navy | Lynch             | 1970.3 | 793              | -274.1        | 85.8          | -64.5          | 82.4                         |
| DSDP15GC  | Scripps | Glomar Challenger | 1970.9 | 180              | -249.2        | 321.2         | 45.6           | 116.6                        |
| U371CB    | USGS    | Pacific Marine    | 1971.6 | 10,296           | -297.6        | 641.1         | -5.9           | 124.4                        |
| CAG711DO  | NOAA    | Researcher        | 1971.7 | 258              | -158.6        | 87.2          | -46.5          | 50.9                         |
| RESEARC   | NOAA    | Researcher        | 1971.7 | 1,291            | -158.3        | 87            | -46.5          | 50.4                         |
| EQUAP72   | NOAA    | Discoverer        | 1972.4 | 151              | -81.4         | 46.5          | -29.9          | 27                           |
| W1932010  | US Navy | Wilkes            | 1972.6 | 5,731            | -560.8        | 684.1         | 1.1            | 151.6                        |
| RC1602    | Lamont  | Conrad            | 1972.7 | 656              | -189          | 69.6          | -62            | 50.2                         |
| V3002     | Lamont  | Vema              | 1973   | 126              | -217          | 90.7          | -73.6          | 70.9                         |
| V3003     | Lamont  | Vema              | 1973   | 247              | -260.5        | 82.2          | -45.4          | 70.1                         |
| RC1612    | Lamont  | Conrad            | 1973.6 | 272              | -218          | 256.1         | -58.1          | 76.1                         |
| RC1613    | Lamont  | Conrad            | 1973.6 | 261              | -175.9        | 205.3         | -0.3           | 96.1                         |
| V3208     | Lamont  | Vema              | 1975.3 | 101              | -278.2        | 369.1         | 37.5           | 181                          |
| DSD44AGC  | Scripps | Glomar Challenger | 1975.9 | 133              | -246          | 0.3           | -93.3          | 66.2                         |
| RC1904    | Lamont  | Conrad            | 1975.9 | 640              | -469.3        | 347.6         | -34.9          | 124.3                        |
| DSDP45GC  | Scripps | Glomar Challenger | 1976   | 640              | -283.5        | 224.6         | -44.2          | 80.6                         |
| DSDP46GC  | Scripps | Glomar Challenger | 1976.1 | 294              | -290.4        | 137.3         | -62.8          | 87.4                         |
| RC1906    | Lamont  | Conrad            | 1976.1 | 345              | -389          | 87.6          | -163           | 134.7                        |
| RC1907    | Lamont  | Conrad            | 1976.2 | 335              | -282          | 71.8          | -101.5         | 84.2                         |
| RC2001    | Lamont  | Conrad            | 1976.4 | 278              | -242.7        | 576.8         | -22.7          | 111                          |
| DSDP51GC  | Scripps | Glomar Challenger | 1976.9 | 690              | -264.4        | 129.5         | -54            | 79.9                         |
| DSDP52GC  | Scripps | Glomar Challenger | 1977.1 | 225              | -226.9        | 98.6          | -68.1          | 72.4                         |
| DSDP53GC  | Scripps | Glomar Challenger | 1977.3 | 243              | -229.6        | 69.8          | -68.2          | 68.1                         |
| RC2102    | Lamont  | Conrad            | 1977.8 | 149              | -106.4        | 266.2         | 43.9           | 79                           |
| INMD02MV  | Scripps | Melville          | 1977.9 | 227              | -358.6        | 414.6         | -28.4          | 141.7                        |

**Table 1**  
*Continued*

| Survey ID                         | Agency     | Ship              | Date        | Number of points       | Data min (nT)        | Data max (nT)        | Data mean (nT)        | Data standard deviation (nT)        |
|-----------------------------------|------------|-------------------|-------------|------------------------|----------------------|----------------------|-----------------------|-------------------------------------|
| A2097L02                          | Woods Hole | Atlantis II       | 1978.1      | 586                    | -207.5               | 51.6                 | -62.9                 | 64                                  |
| RC2109                            | Lamont     | Conrad            | 1978.4      | 134                    | -257.5               | 76.8                 | -115.5                | 73.4                                |
| INMD11AM                          | Scripps    | Melville          | 1978.7      | 91                     | -329.1               | 78.9                 | -70.9                 | 116.6                               |
| INMD12MV                          | Scripps    | Melville          | 1978.7      | 60                     | -273.7               | 33.6                 | -127.3                | 85.4                                |
| KA343904                          | US Navy    | Kane              | 1979.1      | 91                     | -123.5               | 7.9                  | -56.1                 | 33.5                                |
| RC2212                            | Lamont     | Conrad            | 1979.7      | 2,609                  | -339.8               | 722.7                | -6.5                  | 103.2                               |
| D1107L1                           | IOS (UK)   | Discovery         | 1980        | 164                    | -176.3               | 73.5                 | -46.2                 | 68.4                                |
| D1107L2                           | IOS (UK)   | Discovery         | 1980        | 134                    | -82.1                | 23.8                 | -28.3                 | 33.7                                |
| D1107L3                           | IOS (UK)   | Discovery         | 1980.1      | 75                     | -42.5                | 56.2                 | 28.6                  | 22.8                                |
| 80011211                          | IFREMER    | Jean Charcot      | 1980.9      | 156                    | -0.9                 | 110.6                | 48.1                  | 31.1                                |
| DSDP78AC                          | Scripps    | Glomar Challenger | 1981.1      | 547                    | -69                  | 210.4                | 31.1                  | 49.4                                |
| DSDP78BC                          | Scripps    | Glomar Challenger | 1981.2      | 287                    | -264.5               | 169.5                | -32.5                 | 93.2                                |
| DSDP82GC                          | Scripps    | Glomar Challenger | 1981.9      | 393                    | -261.7               | 259.3                | -13.6                 | 81.4                                |
| RC2512                            | Lamont     | Conrad            | 1984.9      | 218                    | -32.2                | 67                   | 5.7                   | 22.3                                |
| RC2605                            | Lamont     | Conrad            | 1985.3      | 14,843                 | -417.8               | 559.9                | 18.7                  | 108.2                               |
| FARN3B85                          | NERC (UK)  | Farnella          | 1985.8      | 68                     | -52.5                | 92.2                 | 14.6                  | 41.1                                |
| FRNL85-4                          | USGS       | Farnella          | 1985.9      | 13,383                 | -415.5               | 687.4                | -18.6                 | 118.4                               |
| 87004711                          | IFREMER    | Jean Charcot      | 1987.9      | 4,764                  | -367                 | 522.7                | -10.5                 | 117                                 |
| 87004712                          | IFREMER    | Jean Charcot      | 1988        | 3,178                  | -275                 | 153.8                | -37                   | 90.9                                |
| ODP149JR                          | ODP        | Joides Resolution | 1993.2      | 1,301                  | -342.1               | 392.7                | -26.8                 | 140.7                               |
| EW9501                            | Lamont     | Ewing             | 1995.1      | 1,399                  | -428.9               | 191                  | -37.8                 | 144.4                               |
| EW9605                            | Lamont     | Ewing             | 1996.5      | 24,526                 | -475.5               | 412                  | -75.3                 | 106.6                               |
| EW9606                            | Lamont     | Ewing             | 1996.5      | 585                    | -223.5               | 172.4                | -66.2                 | 73.2                                |
| 20110030                          | NOAA       | Oceanographer     | 2002.2      | 547                    | -63.9                | 141.8                | 49.4                  | 50.6                                |
| JR340T                            | ODP        | Joides Resolution | 2012.2      | 5,428                  | -32.7                | 130.4                | 70.4                  | 34.1                                |
| JR342T                            | ODP        | Joides Resolution | 2012.4      | 9,421                  | -280.6               | 415.2                | 59.5                  | 192.3                               |
| Overall summary mean/total values |            |                   | Date (mean) | Total number of points | Data min (nT) (mean) | Data Max (nT) (mean) | Data Mean (nT) (mean) | Data standard deviation (nT) (mean) |
| All                               |            |                   | 1988.2      | 128,579                | -560.8               | 722.7                | -11.4                 | 125.5                               |



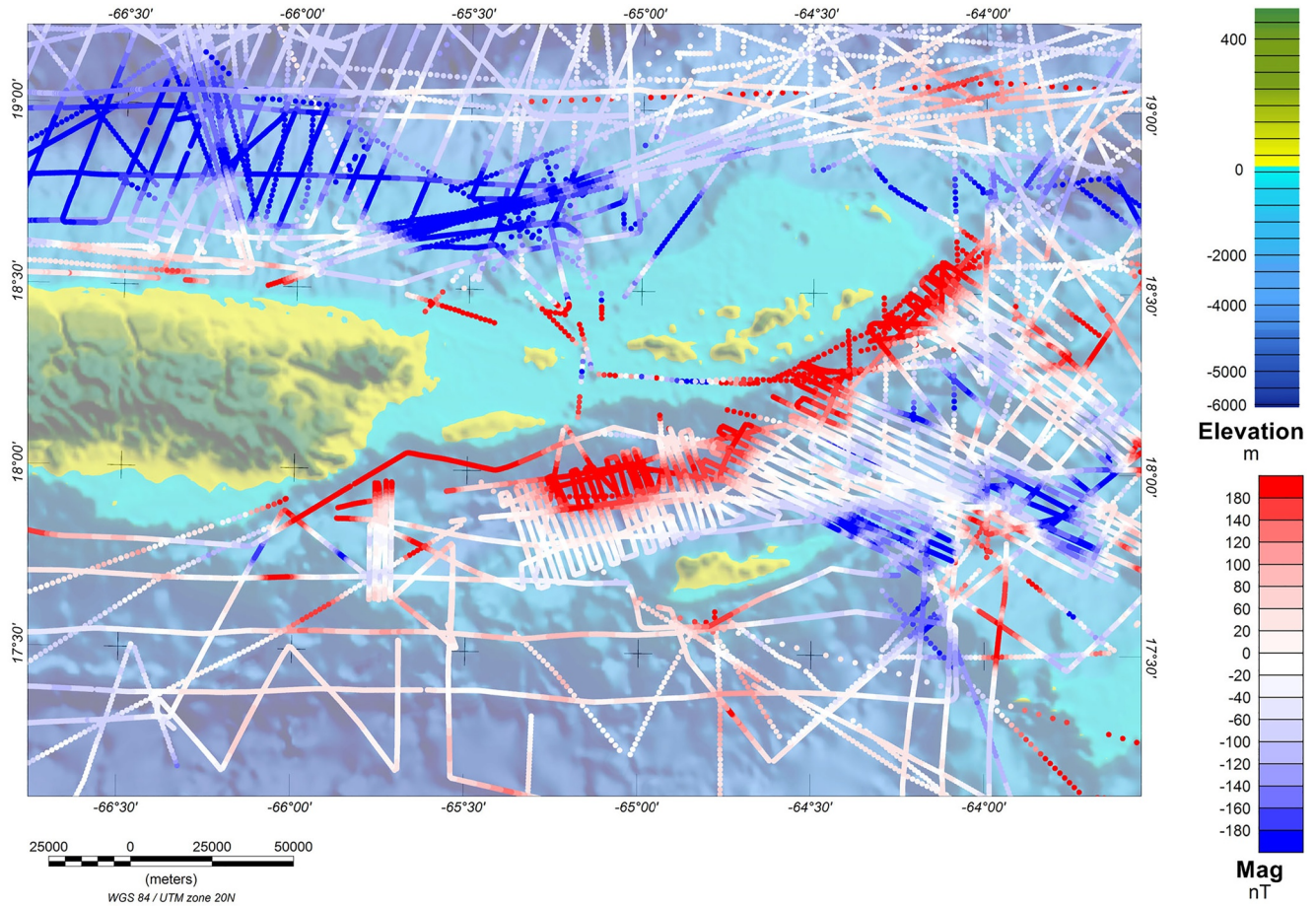


**Figure 2.** Marine trackline data map for the Caribbean Alternative Navigation Reference Experiment central study area. The trackline data are plotted as dots colored by magnetic anomaly values as shown on the color scale at the bottom right. The background is bathymetry/topography from SRTM30 (Becker et al., 2009).

The next step is to define the parameters for the desired data grid ( $x$  and  $y$  limits, grid spacing) and sort the trackline data into bins based on the grid cells, as well as for the 9 subcells with  $1/3$  of the overall grid spacing. The grid coordinates ( $x$ ,  $y$ ) use the UTM20N projection, with grid coordinate values in meters. The  $3 \times 3$  subcells are discussed below, but statistics at the subcell level are not used in the overall calculation of uncertainty. Unless otherwise specified, the summations in the following equations are taken over 1 to  $n$ , where  $n$  is the number of data values within the grid cell.

For each grid cell containing three or more data values we calculate a weighted mean,  $\mu_w$ , based on the standard error propagation formula (e.g., Taylor, 1997):

$$\mu_w = \frac{\sum_{i=1}^n \left( \frac{b_i}{\sigma_i^2} \right)}{\sum_{i=1}^n \left( \frac{1}{\sigma_i^2} \right)} \quad (1)$$

where  $b_i$  are the trackline magnetic anomaly values in the cell and  $\sigma_i$  are their associated uncertainties (listed in Table 2).

The associated uncertainty for this standard weighted mean is then given by:

$$E_m = \sqrt{\frac{1}{\sum_{i=1}^n \left( \frac{1}{\sigma_i^2} \right)}} \quad (2)$$



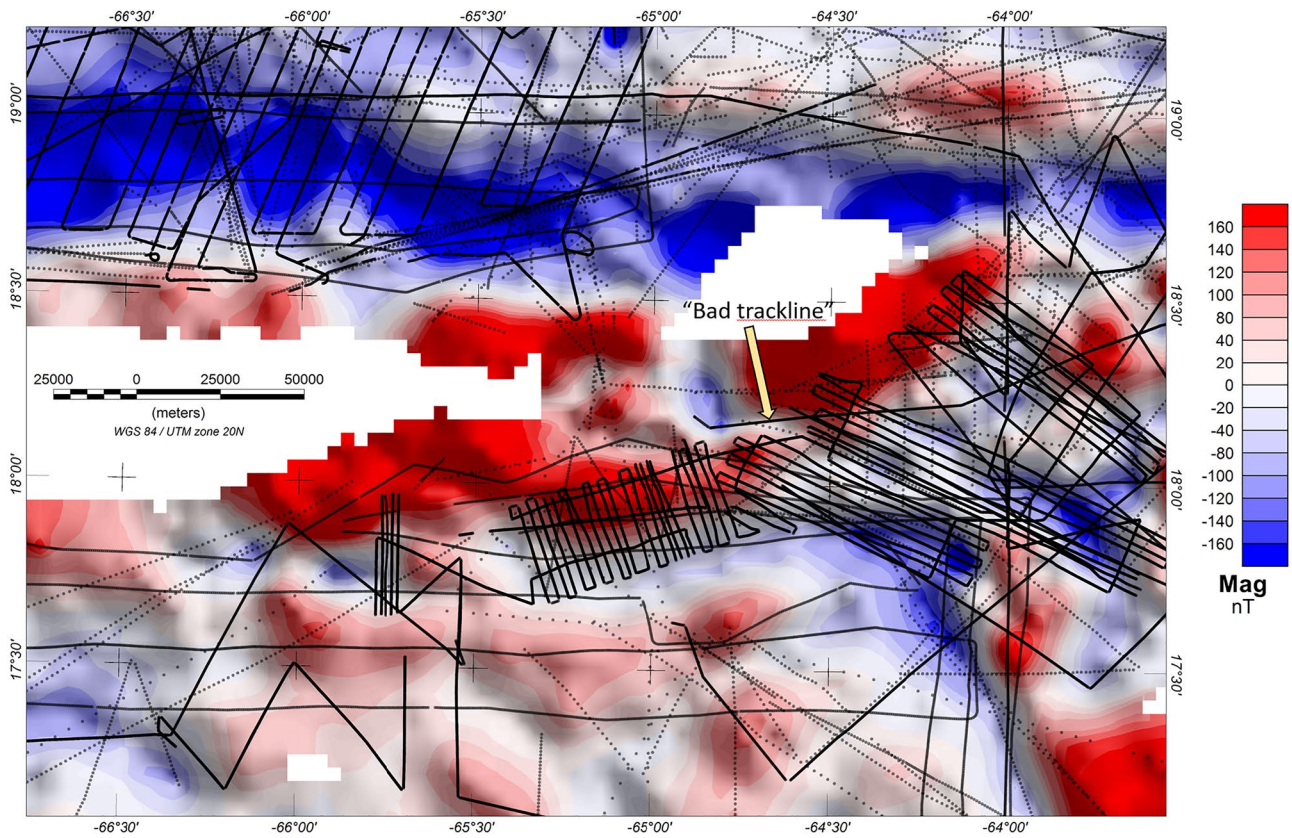


**Figure 3.** Simple kriging grid based directly on the marine trackline data. The trackline labeled as “bad trackline” is discussed later.

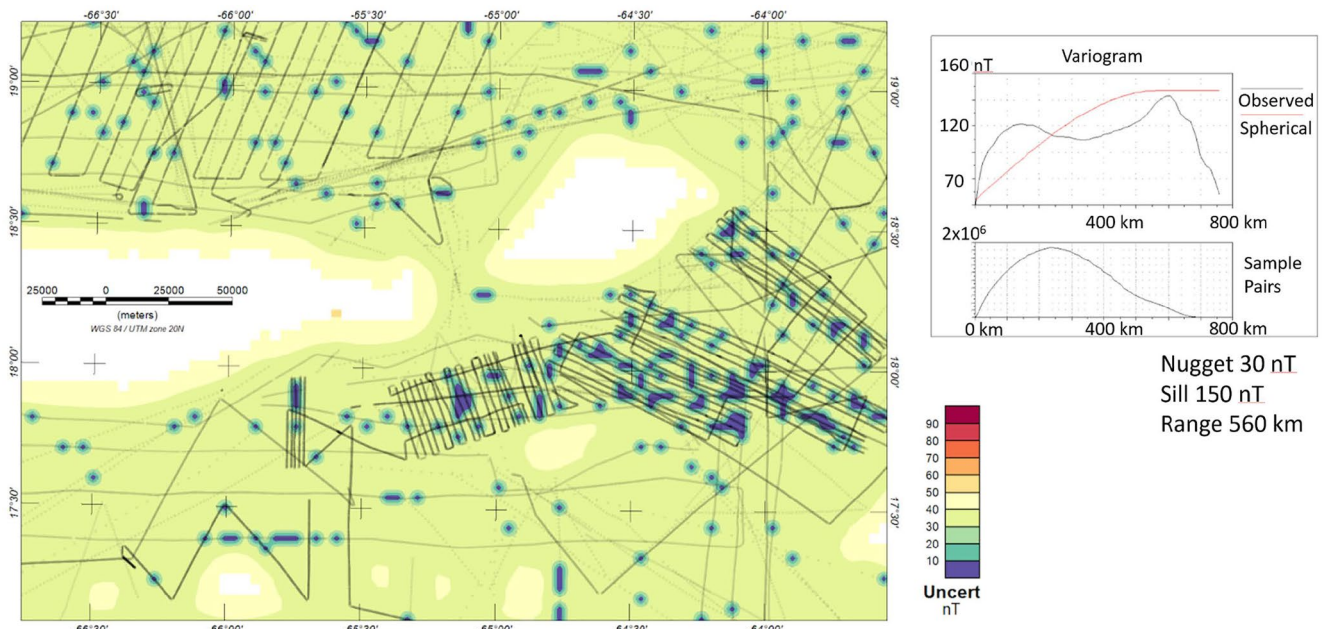


**Figure 4.** Simple uncertainty estimate based directly on the marine trackline data. Inset shows a depiction of the semivariogram model applied.

**Table 2**  
*Assigned Pointwise Uncertainty Based on Survey Year*

| Vintage   | Pt uncertainty (nT) |
|-----------|---------------------|
| Pre 1980  | 40                  |
| 1980–2000 | 20                  |
| Post 2000 | 10                  |

This value,  $E_m$ , is commonly called the “error on the weighted mean,” but we consider it to be a simple estimate of the uncertainty of our weighted mean value relative to the true (but generally unknowable) value for the average magnetic anomaly within the grid cell.

This simple estimate can be easily seen to be incomplete, because it does not take into account factors such as the spatial distribution of the trackline data within the grid cell (e.g., are the values concentrated in one corner of the grid cell or are they well distributed across the cell?), as well as the expected standard deviation of the true magnetic anomaly throughout the cell.

Wang et al. (2014) devised a statistical methodology for estimating grid cell uncertainties that is sensitive to (a) variation in native uncertainty, (b) to expected variability within a grid cell, and (c) to the spatial sampling of the grid cell. Their study focused on measurements of CO<sub>2</sub> concentration, but it can be readily adapted to magnetic anomaly measurements.

Following Wang et al. (2014), the total uncertainty  $\sigma_T$  for a weighted mean value of data within a grid cell is the combination in quadrature of three components:

$$\sigma_T = \sqrt{E_m + \sigma_s^2 + \sigma_u^2} \quad (3)$$

where  $E_m$  is the standard error of the weighted mean discussed above,  $\sigma_s^2$  is the spatial variance, and  $\sigma_u^2$  is the under sampling variance.

For our application  $\sigma_s$  and  $\sigma_u$  are computed as follows:

$\sigma_s^2$  is the variance of the data within the grid cell and is computed as the squared weighted standard deviation of the trackline data points within the grid cell (equation from NIST Dataplot—<https://www.itl.nist.gov/div898/software/dataplot/refman2/ch2/weighvar.pdf>):

$$\sigma_s^2 = \sum_{i=1}^n \left( \frac{\sigma_i(x_i - \mu_w)^2}{\frac{(n-1)}{n} \sum_{i=1}^n \sigma_i} \right) \quad (4)$$

where  $n$  is the number of weighted values in the grid cell and other variables are as defined above.

$\sigma_u^2$  is the under sampling variance (see Wang et al., 2014) which we calculate as follows:

$$\sigma_u^2 = \frac{\sigma_s^2}{f \times n} \quad (5)$$

where  $f$  represents the percentage of the grid cell that is sampled by trackline data. We approximate  $f$  by subdividing the grid cell into  $3 \times 3$  subcells and finding the number of these subcells that contain data points. This number,  $n_{sc}$ , ranges from 1 to 9 and converts to  $f$  as  $f = n_{sc}/9$ . Note that the Wang et al. (2014) definition of  $\sigma_u^2$  has an additional term,  $\alpha$ , that represents the correlation of true value variance within the grid cell. For our implementation we set this term to 1, but future work could investigate the use of a priori magnetic field information to provide an informed value for this parameter.

As given above, the total uncertainty,  $\sigma_T$ , is calculated in standard quadrature which implicitly assumes independence between the combined factors. Of course this is not strictly true as  $\sigma_s$  and  $\sigma_u$  are clearly related. Wang et al. (2014) note this dependence but maintain that the calculated total uncertainty still represents a useful overall representation of expected uncertainty given the information generally available.

The result of this application of the modified Wang et al. (2014) methodology is the assignment of weighted mean ( $\mu_w$ ) and associated total uncertainty ( $\sigma_T$ ) to cells of the study area grid that include measured data. From this stage the kriging methodology is applied to interpolate values into non-data cells and to calculate an uncertainty (usually termed as “error” in kriging application) grid based on the semivariogram applied.

The standard implementation of the kriging methodology requires the definition of a semivariogram function that is applied as spatial weighting of scattered data relative to the position of the value to be estimated. For this study a spherical semivariogram is applied in which the nugget (uncertainty at zero distance) is set to zero (we



have already established the total uncertainty  $\sigma_T$  at each grid cell containing data), the range (the maximum data correlation distance) is set to 100 km, and the sill (the maximum uncertainty reached at the maximum correlation distance) is 120 nT. These values are set based on examination of the semivariograms (e.g., right side of Figure 4) and the use of a spherical equation (Figure 5). The maximum (sill) uncertainty value is consistent with the global marine magnetic grid value uncertainty estimated for EMAG2v3 (Meyer, Chulliat, & Saltus, 2017).

Applying the kriging methodology with these parameters to the set of grid cell weighted mean values results in the anomaly grid and associated uncertainty grid shown in Figure 6.

The interpolation uncertainty grid (Figure 6b) does not take into account the previously calculated point uncertainties related to the grid cell weighted mean values. To combine the calculated and interpolated values we use linear interpolation to fill out the sparse grid of total point uncertainty values and add this grid to the calculated kriging interpolation uncertainty grid. The resulting combined total uncertainty,  $\sigma_{CT}$ , is shown in Figure 7.

The combined uncertainty grid (Figure 7) shows predicted magnetic grid uncertainties ranging from less than 10 nT to greater than 90 nT. The lowest uncertainties occur where there is dense coverage of trackline data of more recent vintage. The highest uncertainties occur at the greatest data gaps (as expected).

#### 4. Validation

A state of the art aeromagnetic survey was conducted to test the magnetic anomaly grid and associated uncertainty values for the CANREx study area. The survey was conducted by Sander Geophysics Ltd. (SGL).

Airborne operations were based out of the International Airport on the island of St. Croix. A Cessna Grand Caravan 208B aircraft, specially modified for aeromagnetic surveying, was employed. Total magnetic intensity (TMI) data were recorded using a Geometrics G-822A non-oriented (strap-down) optically-pumped cesium split-beam sensor mounted in a fiberglass stinger extending from the tail of the aircraft. These magnetometers have a sensor noise of  $0.001 \text{ nT}/\sqrt{\text{Hz}}$  and a range of 20,000 to 100,000 nT. Data were recorded at a rate of 160 Hz, down sampled to 10 Hz during post-mission data processing. Magnetic data were also recorded using a three-axis flux-gate magnetometer at a rate of 10 Hz, used primarily to provide information with which to compensate the TMI for the magnetic effects of aircraft maneuvers in flight. GPS data were recorded from an antenna mounted on the roof of the aircraft at 10 Hz, and used to provide both location and time stamps to all data recorded on a Sander Geophysics Data Acquisition System.

In addition to the airborne data, magnetic and GPS data were acquired at two static reference stations established in magnetically quiet areas at the airport and in the grounds of the hotel where survey crew were accommodated. These data were employed to provide a correction for the diurnal variation of the magnetic field during acquisition, as well as for differential GPS corrections that locate the aircraft to within 1 m. GPS time provided precise synchronization of the data from the airborne and reference systems.

A total budget of 5,000 line kilometers of airborne survey was spread over four individual but partially overlapping blocks designated A to D (Figure 8). All data were acquired offshore in order to specifically target testing of marine survey data. The four blocks were located so as to provide data in areas with different characteristics in the manner in which the marine data was acquired, while also taking into account areas of different geological settings and associated magnetic anomaly patterns.

#### Spherical Model

$$\gamma(h) = \begin{cases} C_0 + C \left[ \left( \frac{3h}{2a} \right) - 0,5 \left( \frac{h}{a} \right)^3 \right] & \text{for } h \leq a \\ C_0 + C & \text{for } h > a \end{cases}$$

where:

$h$  = distance of sample location

$C_0 + C$  = sill, the semivarogram value for distances when magnitude is constant

$a$  = range, the distance when the semivogram value reaches sill

**Figure 5.** Canonical form of the spherical model used in kriging (Nur'eni et al., 2020).

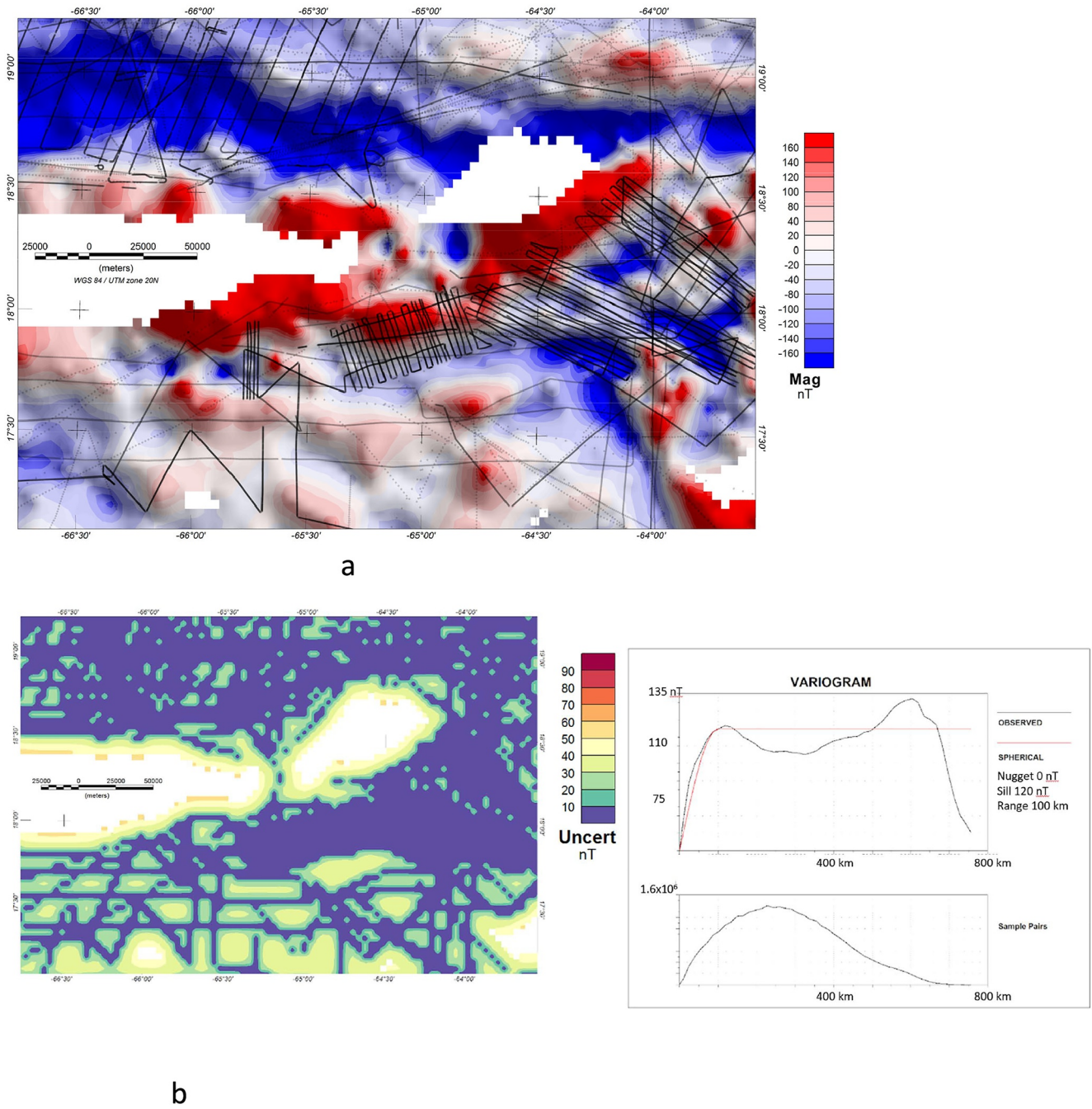


**Figure 6.** Kriging grids: (a) Kriging grid based on weighted average cell values, (b) Calculated kriging interpolation uncertainty for the weighted average grid.

Since the EMAG2 is rendered on a 4 km grid spacing, close survey line spacing was not considered optimal use of the line kilometer budget. Priority was given to obtaining data from as many different cells as possible. Survey line directions were selected mainly for operational efficiency, although, for Block A in particular, survey lines were designed to follow the trend of specific widely spaced marine track lines. A certain number of perpendicular tie-lines were also flown in each block to provide leveling corrections to remove residual diurnal magnetic effects from the data. Details for each Block are provided in Table 3.

In general there were no restrictions on flying at the survey altitude, except for a military zone at the west end of Block A that was avoided. Two lines of Block C were extended to the north-northwest toward Block B to provide ferry guidance between islands.

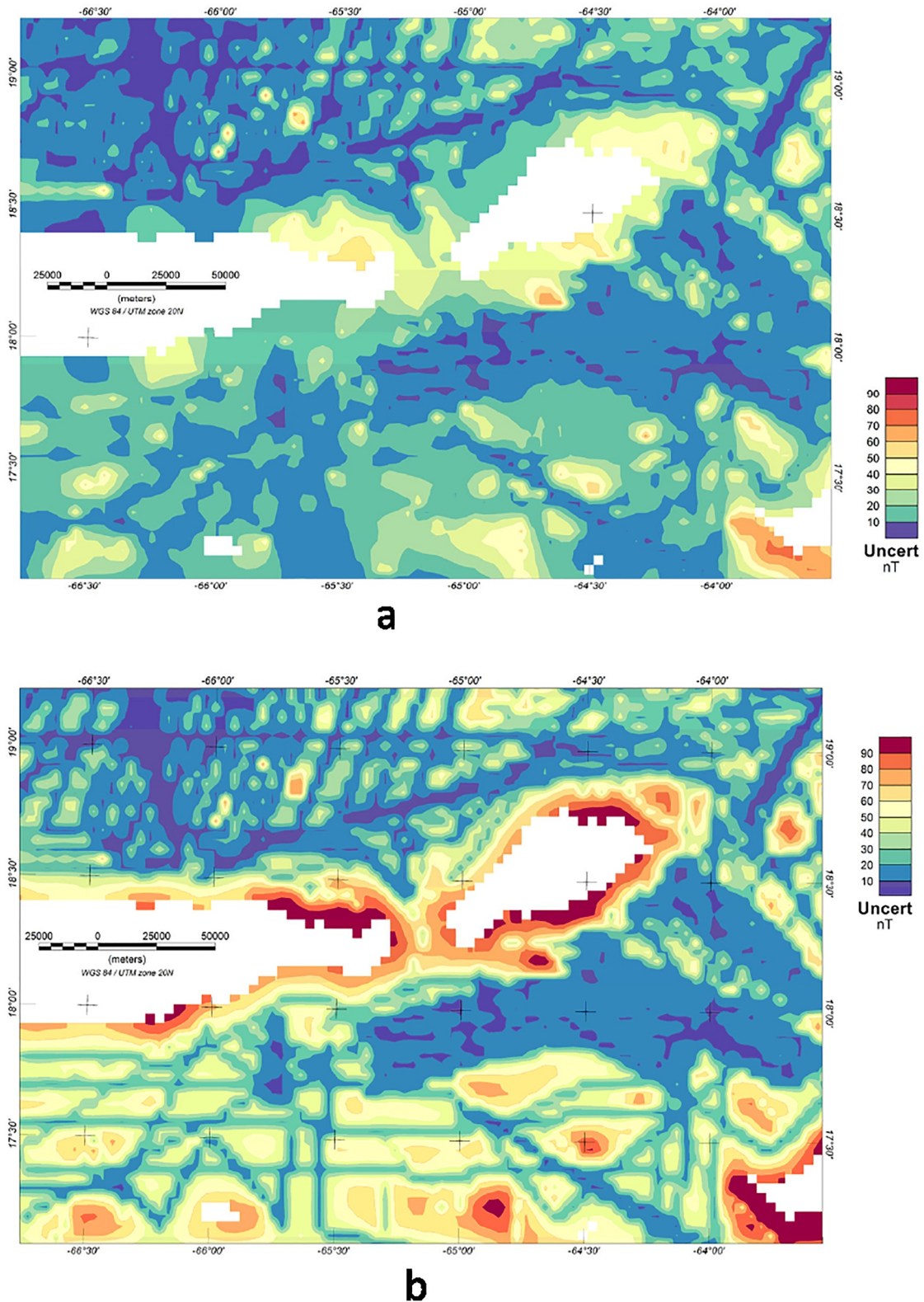


**Figure 7.** (a) Linear interpolation of total point uncertainty. (b) Combined uncertainty grid (total point uncertainty plus interpolation uncertainty shown in Figure 6). Note that a larger blanking distance was used for interpolation of the total point uncertainty (a) to ensure complete coverage for summation with the kriging uncertainty to produce the total uncertainty shown in (b).



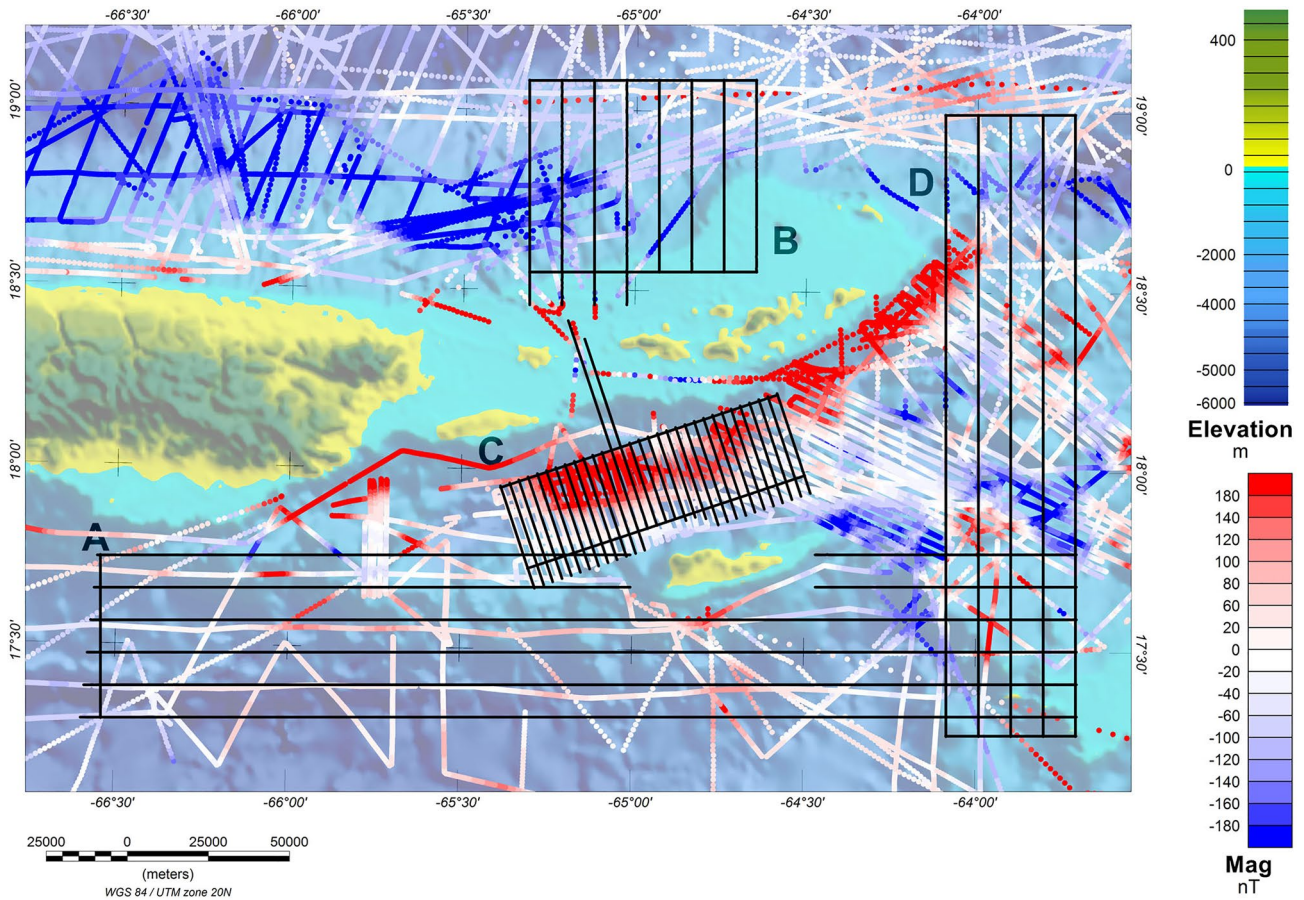


**Figure 8.** Map of the Sander Geophysics Ltd. Caribbean Alternative Navigation Reference Experiment survey (black lines). See text for discussion. Colored lines depict the trackline magnetic data in the region (see also Figure 2). Background is colored bathymetry.

Survey flights of up to 6.5 hr were performed at a target speed of 135 Knots. The target altitude was 300 m above mean sea level. This altitude was selected so as to be close to the ocean surface where marine data were acquired, without posing an undue safety risk. Five lines were re-flown at 1,830 m (6,000 feet) in blocks C and D to provide data on variation of signal with altitude.

Magnetic variations at the static reference stations were monitored throughout the survey to ensure that data flights were not conducted during periods of large diurnal variation. Total field values were reduced to magnetic anomaly values by subtraction of reference values from the 2020 IGRF calculated for the period of the magnetic survey.

The SGL CANREx aeromagnetic survey is regarded as “truth” for the evaluation of the marine trackline map and uncertainty model. Of course there is still some uncertainty in even the most modern survey, but the use of high precision GPS navigation, a dedicated survey aircraft, local magnetic base station corrections, etc., yields confidence in the results at the  $\pm 1$  nT level (e.g., Fairhead et al., 2017), particularly for defining magnetic anomalies at our relatively broad test grid spacing of 4 km.

**Table 3**  
Specifications of the Sander Geophysics Ltd. Caribbean Alternative Navigation Reference Experiment Survey

| Block name | Line spacing (km) | Line direction |
|------------|-------------------|----------------|
| A          | 10                | East           |
| B          | 10                | North          |
| C          | 3                 | North 20° West |
| D          | 10                | North          |

The SGL CANREx aeromagnetic profiles track very well to the anomaly predictions from the marine trackline grid (Figure 9). To quantify the performance of the marine trackline map and uncertainty model relative to the validation survey, we extracted anomaly and uncertainty information from the model grids along the airborne survey flightlines. The airborne survey magnetic anomalies were filtered using a 4 km rolling average to enable direct comparison with the 4 km grid spacing of the trackline models. Error of the

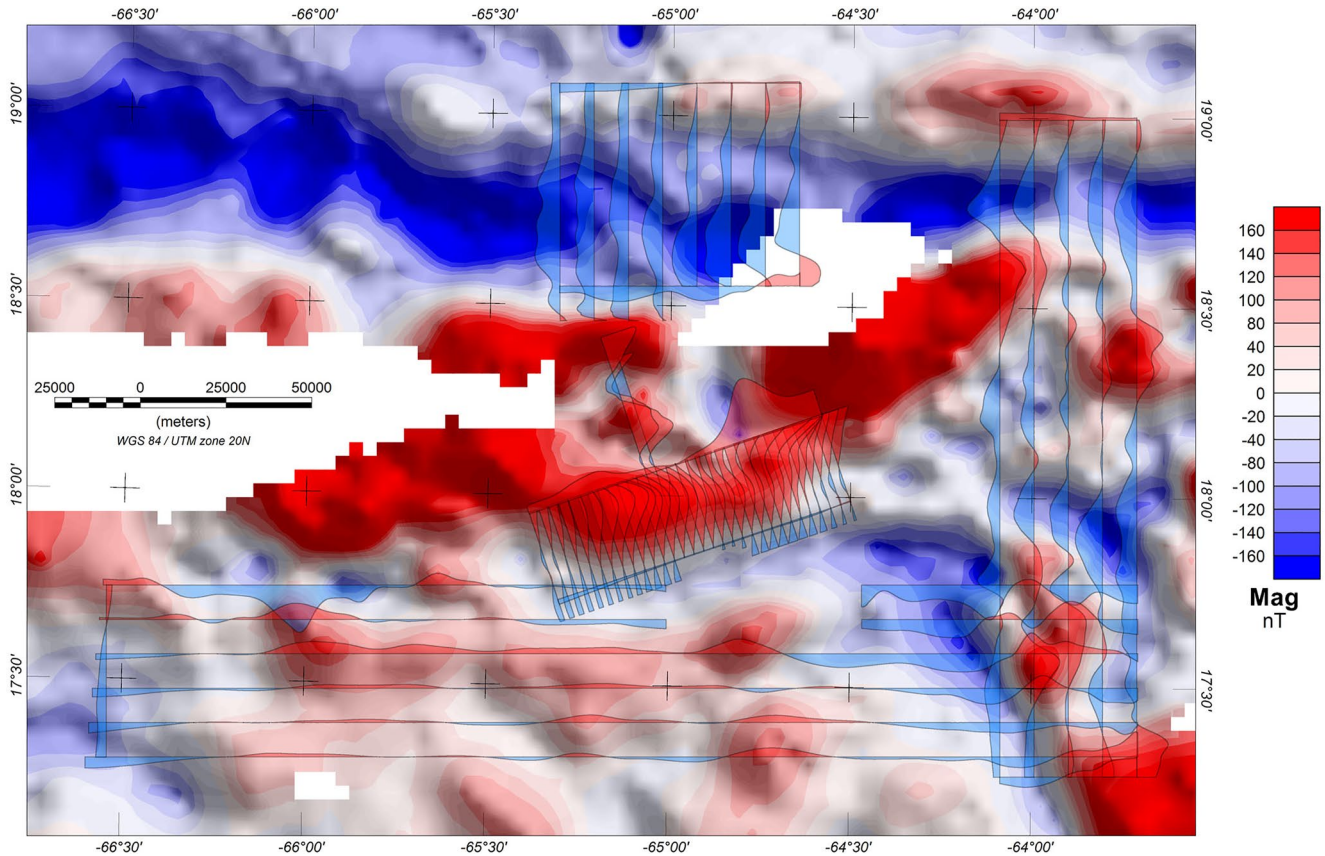


**Figure 9.** Map comparing the gridded marine trackline magnetic anomalies overlain by the Sander Geophysics Ltd. Caribbean Alternative Navigation Reference Experiment aeromagnetic profiles.

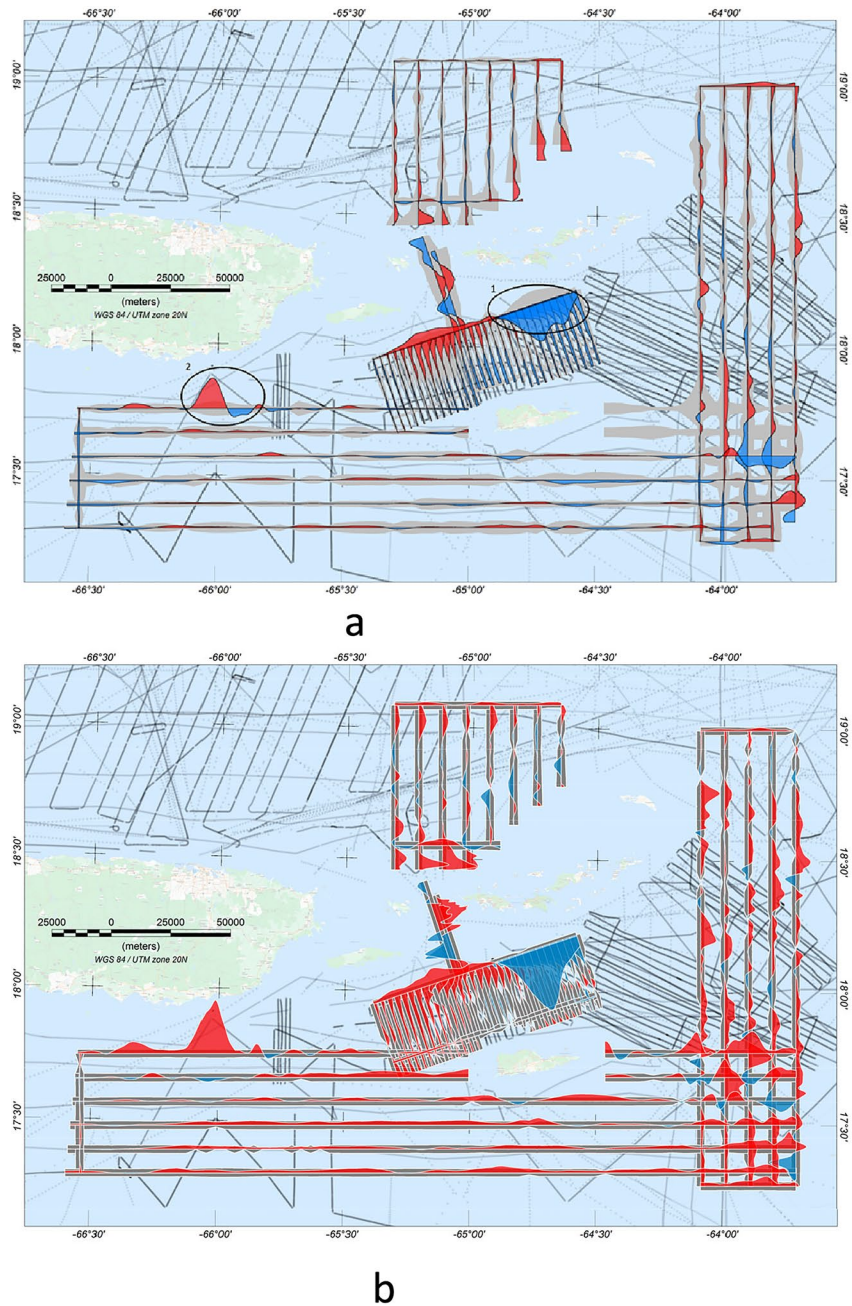
trackline magnetic grid relative to the airborne survey is defined as  $\epsilon = m_T - m_S$ , where  $m_S$  is the SGL CANREx magnetic anomaly (truth) and  $m_T$  is the magnetic anomaly from the marine trackline grid. A useful metric for tracking the quality of the uncertainty model is  $\eta$  calculated as  $\frac{\epsilon}{\sigma_{CT}}$ . Quality ( $\eta$ ) values between +1 and -1 represent success of the uncertainty model (i.e., error falls within the bounds of uncertainty). Since the uncertainty calculations and definitions implicitly define predicted 1 sigma error, a standard deviation of about 1 for the quality metric is considered a successful outcome.

Figure 9 shows a profile depiction of the SGL aeromagnetic profiles superimposed on the marine trackline anomaly grid. Visual inspection shows the general agreement of the SGL profile magnetic anomaly values with the gridded trackline map patterns. Figure 10a shows a map depiction of the 1 sigma ( $|\text{abs}\eta| \leq 1$ ) uncertainty model (gray shading) compared with the error (truth minus model) difference between the SGL measured profiles and the marine trackline grid. This metric is met on 71% of the flightline distance. For comparison, a similar display for the default kriging uncertainty estimate (discussed previously) is shown in Figure 10b. The default kriging uncertainty estimate also meets the 1 sigma ( $|\text{abs}\eta| \leq 1$ ) criteria on about 71% of the flightline distance, however, as discussed further below, the full uncertainty model (Figure 10a) includes more dynamic variability, better reflecting patterns in the observed errors.

Overall we judge the model to be successful at the one sigma level. It is useful, however, to examine the portions of test flightlines where the error significantly exceeds the uncertainty estimate. The two greatest mismatches are labeled 1 and 2 on Figure 10a. We consider these two examples (Figures 11 and 12).

At location 1, a single mis-leveled trackline (upper right panel, Figure 11) shows anomaly values that are systematically lower than surrounding and crossing flightlines. This trackline traverses an open region with no other tracklines. The combination of this geometry and the systematic offset of the data values relative to the adjoining tracklines skews the weighted average in this region of the grid. This model failure would be corrected if more





**Figure 10.** Maps comparing error (difference between Sander Geophysics Ltd. (SGL) aeromagnetic profiles and predicted anomalies from trackline grids) relative to the uncertainty estimate (gray shading) for the trackline grid. Positive (red shading) error indicates the grid value is greater than the SGL profile value. Negative (blue shading) indicates the grid value is less than the SGL flightline value. Labeled ovals (1 and 2 on a) show the location of large error excursions beyond the modeled uncertainty (see text for discussion). (a) Results for weighted average grid values and total uncertainty values. (b) Results for default kriging of trackline data and default kriging uncertainty.

care was taken with initial quality control prior to statistical calculations and gridding, if the data values from this trackline had been assigned a significantly larger point uncertainty (based on factors in addition to year of survey), or if line crossing differences were used for survey to survey or line to line leveling adjustments.

At location 2, Figure 12 shows that a central data gap is surrounded on the north and south by high data values and on the east and west by low data values. The SGL survey shows that a better representation of the magnetic



### USVI data analysis – isolated gridded data issue #1

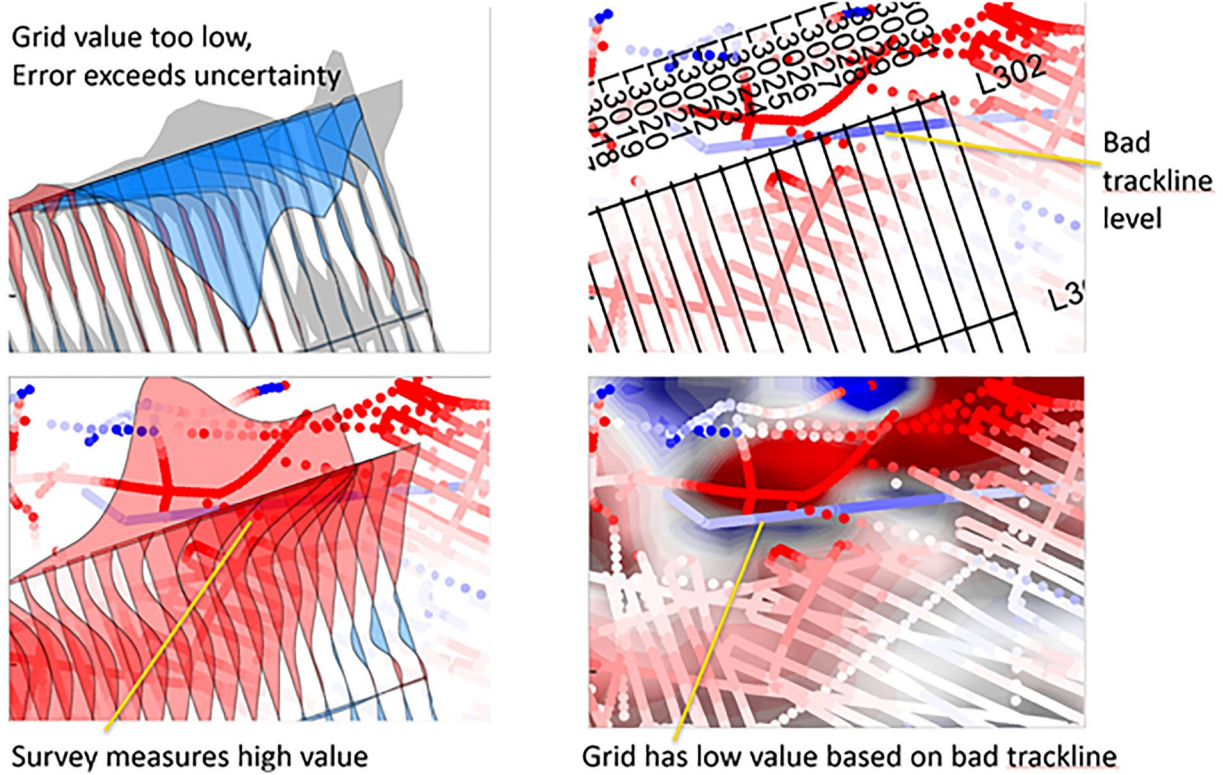


**Figure 11.** Illustration of model failure at location 1. Upper left panel shows the error and uncertainties, like in Figure 10a. Upper right shows the actual trackline values. Lower left shows profiles of survey data superimposed on the trackline data. Lower right panel compares the trackline values to the marine trackline grid (smoothed from the original 4 km cell size for display at this resolution). The location of the “bad trackline” is also shown on Figure 3.

### USVI data analysis – isolated gridded data issue #2

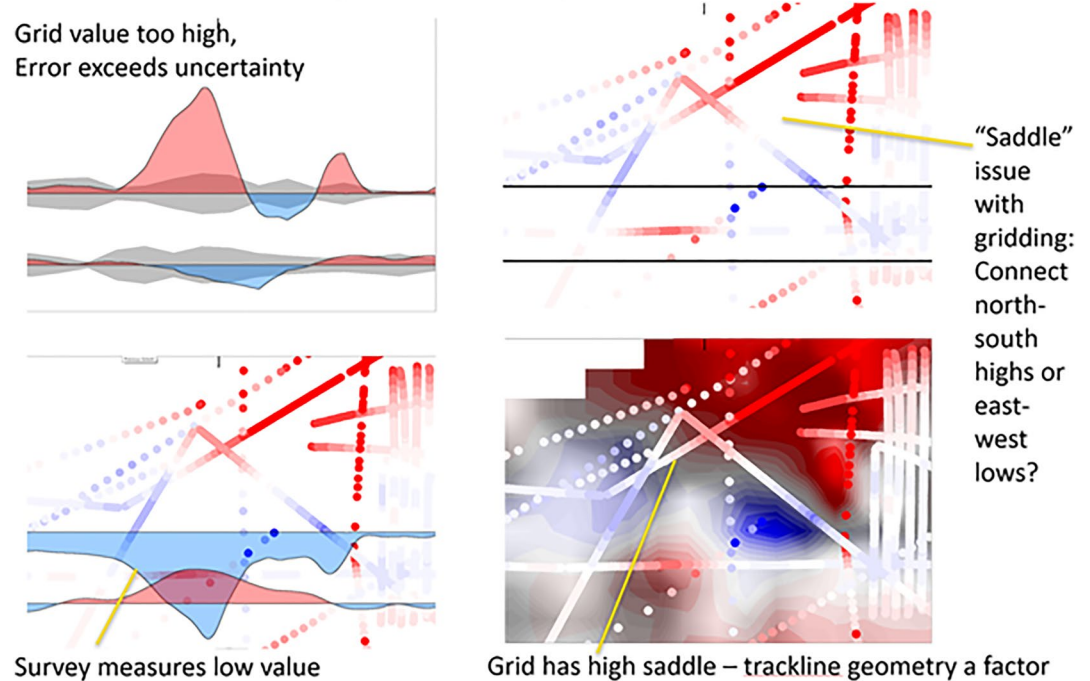


**Figure 12.** Illustration of model failure at location 2. See caption to Figure 11 for explanation of the panel contents.

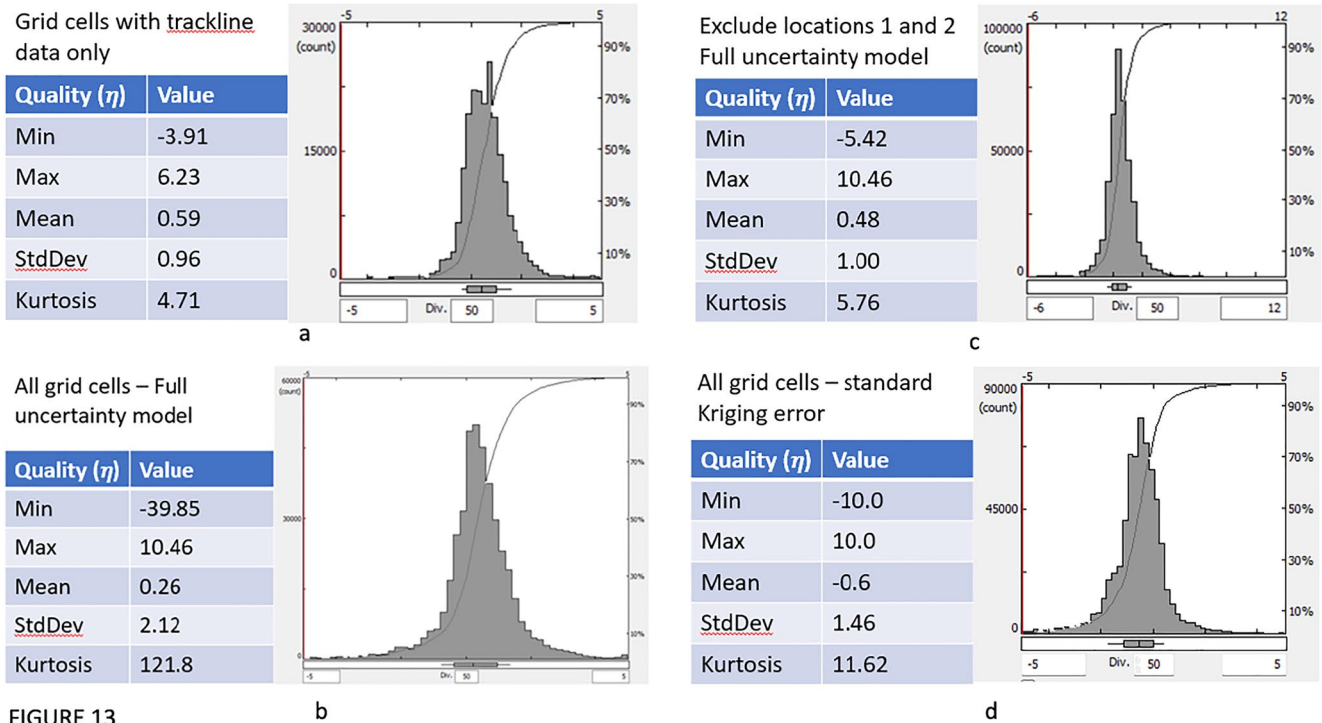


**FIGURE 13.** Histogram analysis of quality ( $\eta$ ) of the trackline anomaly and uncertainty model relative to the Sander Geophysics Ltd. (SGL) Caribbean Alternative Navigation Reference Experiment validation survey; (a) Statistics and histogram distribution for SGL survey lines crossing grid cells with intersecting marine tracklines; (b) Statistics and histogram distribution for the full SGL survey lines crossing both grid cells with intersecting marine tracklines and interpolated grid cells; (c) Same analysis as panel (b) except that data from locations 1 and 2 (locations on Figure 10) are excluded. (d) Statistics for default application of the kriging algorithm directly to trackline data (see also Figure 4).

anomaly in this area would follow an east-west trend and carry the low data values through this data gap. Absent trend guidance, the kriging algorithm splits the difference between the high north-south trend and the low east-west trend to create a saddle in the grid surface. This model failure could be corrected by including predicted trend information (e.g., a priori expectation from bathymetric trends or geologic environment) in the gridding operation.

As a measure of the overall effectiveness of the uncertainty model relative to the SGL survey, four statistical summaries are shown in Figure 13. The first summary (Figure 13a) shows statistical comparison of error divided by uncertainty for the trackline marine grid cells that are traversed by at least one trackline. In these cells the grid value is the calculated weighted mean of the data in the cell. The uncertainty value in these cells is equal to the three component “Wang” uncertainty calculated following our implementation of the methodology of Wang et al. (2014). Optimum statistical behavior of the uncertainty model would result in a standard deviation less than or equal to 1 and a kurtosis close to 1. Figure 13a shows a standard deviation of 0.96 and a kurtosis of 4.7. The standard deviation is optimal, the kurtosis is greater than 1 which indicates a slightly non-Gaussian form to the histogram “bell” shape.

The second summary (Figure 13b) shows the statistical results for all marine trackline cells traversed by the SGL survey. The grid values for these cells are roughly 1/2 based on direct calculation of weighted mean and 1/2 based on the kriging interpolation of anomaly values into cells not directly constrained by data. This test includes the two known problem locations discussed above and shown in Figures 11 and 12. In this case the overall model behavior is slightly suboptimal: the standard deviation of error divided by uncertainty is 2.1 and the kurtosis is about 122. This demonstrates the large statistical significance of a relatively small zone of model failure.

If the two “outlier” zones are excluded from the analysis, the statistical results are once again optimal (Figure 13c). Here the standard deviation is very close to 1 and the kurtosis is about 5. The error values skew slightly positive relative to a Gaussian distribution. This indicates the general effectiveness of the model with the caveat that the

ability to effectively estimate uncertainty is degraded in interpolated regions of the data grids. This is, of course, no surprise: one is always better off in regions of data versus regions of no data.

Figure 13d shows the performance of the default kriging methodology applied directly to the leveled trackline magnetic data (i.e., similar gridding approach as that taken in the construction of EMAG2v3; Meyer, Chulliat, & Saltus, 2017). As shown previously (Figure 10b), the uncertainty model created under the default (large range of covariance influence) kriging parameters produces a relatively uniform uncertainty distribution. This uncertainty model produces, on average, a reasonable performance ( $\eta \approx 1.5$ ), but does not capture the regional variations in uncertainty as well as the combined Wang plus kriging methodology.

## 5. Conclusions and Recommendations

We conclude that a hybrid data gridding approach, combining the three component methodology of Wang et al. (2014) for data cells containing data and a standard kriging methodology for interpolated cells, allows for construction of useful grids with associated uncertainties when applied to marine magnetic trackline data. A test of this methodology in the area surrounding the USVI demonstrates nominal performance within this study area at the model resolution used for the EMAG2 grids (i.e., 4 km grid spacing at low latitudes). It is worth noting that even the default uncertainty estimates using the kriging approach provide a reasonable first approximation of uncertainty in the absence of further analysis. This will be particularly true in marine regions of very sparse data coverage as the primary source of uncertainty in these regions is the distance to nearest measured data values.

The 4 km grid spacing used in this study conforms to the two-arc min spacing of the EMAG2 grids. The calculated cell statistics and derived total cell uncertainty are, of course, in reference to the mean value of the magnetic anomaly within the 4 km grid cell. Larger grid cell spacing would lead to a smoothing of these mean values, and a smaller grid cell spacing would lead to potentially a greater variation in mean values. As mentioned above, the distance to the magnetic sources beneath the seafloor in this region guarantee that the true magnetic anomalies will be smooth at the 4 km scale, so we don't believe the uncertainty would differ significantly for smaller grid cell sizes. However, smaller grid cells would result in generally fewer measured values per cell, which, in turn, would result in less robust statistical measures. Larger grid cells will produce a smoother set of grid cell mean values and generally lower estimates of uncertainty because the values would be constrained by more data. It is important to keep in mind that the uncertainty estimates are relative to mean cell values, not to the "omission error" relative to finer scale field variations within the grid cell.

The method is dependent on the ability to (a) provide reasonable point uncertainties for the original marine trackline observations and (b) define a representative semivariogram for kriging. Both of these tasks require some a priori understanding or estimation of the data quality and expected magnetic field variations in a given area. In detail it is impossible to predict or assess every factor contributing to uncertainty for a given marine survey, particularly for older surveys lacking sufficient metadata. Despite this limitation it appears, based on this initial test, that it is possible to produce magnetic anomaly maps with reasonable and quantifiable accuracy for marine regions with sufficient trackline data density.

A known deficiency of this methodology for broader regional application is the use of a single semivariogram for the full study area. This implies common statistical behavior of the magnetic anomaly field throughout the area, but, due to the irregular distribution of magnetic sources in the crust, a more general solution will require segmentation of the study region into domains with common statistical behavior or the use of a more flexible interpolation methodology such as localized kriging or optimal interpolation (e.g., Melnichenko et al., 2016).

Current use of magnetic map information in navigation simulation for development of alternative navigation generally assigns either no uncertainty or a uniform standard deviation to the magnetic reference map (e.g., Canciani, 2016; Canciani & Raquet, 2016). This assumption is likely reasonable when working with dedicated, modern surveys/maps. However, the need for alternative navigation in remote marine regions will require, in most cases, the use of maps based on the variable quality marine trackline data for those regions. In this case, effective use of this information in navigation (or, as constraints to geological interpretation or inversion) will require knowledge or estimation of the map uncertainty, such as that developed in this paper.



## Data Availability Statement

The marine trackline data used for creating the marine magnetic anomaly grid in the study and the SGL airborne survey lines are available at <https://www.ncei.noaa.gov/products/marine-trackline-geophysical-data> via public access data delivery with no restrictions.

Custom built python code was used for calculation of cell by cell statistics using the formulas given in this paper (Balmes, 2023). This software is preserved at <https://doi.org/10.5281/zenodo.8404375>, available via download for academic use only.

The proprietary software package, Oasis montaj (<https://www.sequent.com/products-solutions/geosoft-oasis-montaj/>) was used for trackline data organization and using tools in the channel math and gridding toolkits, including the Geosoft kriging function. This software is available from Sequent with special rates available for academic use.

## Acknowledgments

We appreciate discussions and ideas from Chris Amante (CIRES/NOAA), the full CIRES/NOAA GeoMag Team, colleagues from the Air Force Institute of Technology and the Penn State Applied Research Lab. The SGL field crew did a great job with the data collection for this project. This research was supported, in part, by Office of Naval Research (ONR) Grant N00014-20-1-2483 and by NOAA cooperative agreement NA17OAR4320101.

## References

- Amante, C. (2018). Estimating coastal digital elevation model uncertainty. *Journal of Coastal Research*, 34(6), 1382–1397. <https://doi.org/10.2112/jcoastres-d-17-00211.1>
- Balmes, A. (2023). CIRES-Geomagnetism/CANREx-Paper: CANREx-Paper-v1 (v1.0) [Software]. Zenodo. <https://doi.org/10.5281/zenodo.8404375>
- Becker, J. J., Sandwell, D., Smith, W., Braud, W., Binder, B., Fabre, D., et al. (2009). Global bathymetry and elevation data at 30 arc seconds resolution: SRTM30\_PLUS. *Marine Geodesy*, 32(4), 355–371. <https://doi.org/10.1080/01490410903297766>
- Canciani, A. (2016). *Absolute positioning using the Earth's magnetic anomaly field* (Ph.D. thesis). Air Force Institute of Technology. Retrieved from <https://scholar.afit.edu/etd/251/>
- Canciani, A., & Raquet, J. (2016). Absolute positioning using the Earth's magnetic anomaly field. *Journal of the Institute of Navigation*, 63(2), 111–126. <https://doi.org/10.1002/navi.138>
- Fairhead, J. D., Cooper, G. R. J., & Sander, S. (2017). Advances in airborne gravity and magnetics. In V. Tschirhart & M. D. Thomas (Ed.), *Proceedings of exploration 17: Sixth decennial international conference on mineral exploration* (pp. 113–127).
- Kolster, M. E., Dössing, A., & Abbas Khan, S. (2023). Satellite magnetics suggest a complex geothermal heat flux pattern beneath the Greenland ice sheet. *Remote Sensing*, 15(5), 1379. <https://doi.org/10.3390/rs15051379>
- Korhonen, J. V., Fairhead, J. D., Hamoudi, M., Hemant, K., Lesur, V., Mandea, M., et al. (2007). *Magnetic anomaly map of the world, scale 1:50,000,000* (1st ed.). Geological Survey of Finland.
- Lesur, V., Hamoudi, M., Choi, Y., Dymont, J., & Thébaud, E. (2016). Building the second version of the world digital magnetic anomaly map (WDMAM). *Earth Planets and Space*, 68(1), 27. <https://doi.org/10.1186/s40623-016-0404-6>
- Melnichenko, O., Hacker, P., Maximenko, N., Lagerloef, G., & Potemra, J. (2016). Optimum interpolation analysis of Aquarius sea surface salinity. *Journal of Geophysical Research: Oceans*, 121(1), 602–616. <https://doi.org/10.1002/2015JC011343>
- Meyer, B., Chulliat, A., & Saltus, R. (2017). Derivation and error analysis of the earth magnetic anomaly grid at 2 arc min resolution version 3 (EMAG2v3). *Geochemistry, Geophysics, Geosystems*, 18(12), 4522–4537. <https://doi.org/10.1002/2017GC007280>
- Meyer, B., Saltus, R., & Chulliat, A. (2017). *EMAG2v3: Earth magnetic anomaly grid (2-arc-minute resolution). Version 3*. NOAA National Centers for Environmental Information. <https://doi.org/10.7289/V5H70CVX>
- Nur'eni, J., Setiawan, I., & Suaib, N. M. (2020). Estimation of ordinary kriging parameters for determining characteristics and distribution of groundwater layer in Tondo area, Mantikulore district, PaluJ. In *Physics: Conference series 1434 012025*.
- Saltus, R., Chulliat, A., Meyer, B., & Amante, C. (2020). Uncertainty quantification for magnetic field maps and models. In *AGU fall meeting 2020, NG002-0013 (abstract)*.
- Saltus, R., Chulliat, A., Meyer, B., & Amante, C. (2021a). Uncertainty estimation for magnetic maps. In *EGU general assembly 2021*. <https://doi.org/10.5194/egusphere-egu21-3541>
- Saltus, R., Chulliat, A., Meyer, B., & Bates, M. (2021b). Towards a quantification of uncertainty in magnetic maps and models. In *AGU fall meeting 2021, NS25A-0421 (abstract)*.
- Taylor, J. R. (1997). *An introduction to error analysis: The study of uncertainties in physical measurements* (2nd ed.). University Science Books.
- Wang, G., Dai, M., Shen, S. S. P., Bai, Y., & Xu, Y. (2014). Quantifying uncertainty sources in the gridded data of sea surface CO<sub>2</sub> partial pressure. *Journal of Geophysical Research: Oceans*, 119(8), 5181–5189. <https://doi.org/10.1002/2013JC009577>